Available online at www.sciencedirect.com

ScienceDirect

IFAC PapersOnline CONFERENCE PAPER ARCHIVE

IFAC PapersOnLine 58-11 (2024) 69–74

Hybrid Optimal Control of a Flying+Sailing Drone: Flying with 6 and Sailing with 5 Degrees of Freedom

Taha Yasini * **Ali Pakniyat** *

* *Department of Mechanical Engineering, University of Alabama, Tuscaloosa, AL, USA*

(e-mails: tyasini@crimson.ua.edu, apakniyat@ua.edu).

Abstract: This paper studies a multi-modal robotic system referred to as a flying+sailing drone with the consideration of six degrees of freedom (6-DoF) for flying and 5-DoF for sailing, i.e., a twelve-dimensional state space for flying and a ten-dimensional state space for sailing. Key characteristics of hybrid systems emerging in tasks involving both flying and sailing are (i) changes in the dimension of the state space as the system switches from flying to sailing and vice versa, (ii) the presence of autonomous switchings triggered upon the landing of the drone on the water surface, and (iii) non-identity jumps in the state upon switching. For the scenario in which the drone's initial state is in the flying mode and a fixed terminal state is specified in the sailing mode, the associated optimal control problems are studied for the minimization of time and the minimization of the control effort. The necessary optimality conditions are obtained from the Hybrid Minimum Principle (HMP), and the associated numerical simulations are presented.

Keywords: Optimal control of hybrid systems, Hybrid and switched systems modeling, Control design for hybrid systems, Hybrid Minimum Principle, Flying+sailing drone.

1. INTRODUCTION

Over the past few decades, the need for multi-modal autonomous robotics systems has emerged in several civil, commercial, and military applications. As, for instance, remarked by (Ackerman, 2022), for quick and efficient military organizations, there is a grave need for a combined robotic system capable of providing services of energy-efficient but slow-moving ships combined with fast but energy-consuming planes. As another example, a multi-modal robotic system inspired by animals and capable of walking and flying is presented in (Sihite et al., 2023). The emergence of these multi-modal control systems calls for the development of fast and efficient control synthesis algorithms capable of handling the "hybrid" nature of these systems. Moreover, fulfilling requirements such as the minimization of time and the minimization of energy consumption in performing the tasks is a significant aspect of the control synthesis in several applications, e.g., in the search and rescue of humans in coasts, where quick human detection is vital (Qingqing et al., 2020; Ho et al., 2022).

In past work of the authors (Yasini and Pakniyat, 2023), a hybrid systems formulation for the planar motion of a drone capable of both flying and sailing is established and solutions to the associated hybrid optimal control problems are presented. This paper extends upon that work by permitting both in-plane and out-of-plane motions for the flying+sailing drone with the consideration of 6-DoF for flying and 5-DoF for sailing. This elaborates on the hybrid systems formulation to represent the flying dynamics in a twelve-dimensional state space and the sailing dynamics in a ten-dimensional state space. For this elaborated formulation, we present and solve the hybrid optimal control problems for time and control effort minimization in a scenario with the system's initial condition provided in the flying mode and a fixed desired terminal condition in the sailing mode which, necessarily, requires the drone to switch from flying to sailing at an intermediate time during its motion. This switching is possible only when the drone reaches the water surface and, hence, it constitutes an autonomous switching. Upon switching the dynamics from flying to sailing, the dimension of the state space necessarily changes as the drone's motion becomes restricted to the water surface.

Theoretical foundations of this work rely on the Hybrid Minimum Principle (HMP) which has been extensively researched in the control theory literature (Shaikh and Caines, 2007; Pakniyat and Caines, 2016, 2017a, 2021, 2023) and, in particular, the version of the HMP with explicit expressions of the boundary conditions for the Hamiltonians and adjoint processes (Pakniyat and Caines, 2021, 2023). The HMP-based multiple autonomous switching (HMP–MAS) algorithm (Shaikh and Caines, 2007; Pakniyat and Caines, 2021), which has been tailored in (Yasini and Pakniyat, 2023) for the in-plane motion of the flying+sailing drone is also extended in this work for general out-of-plane motions.

The structure of the article is as follows. Section 2 presents the hybrid optimal control formulation of the 6-DoF and 5-DoF of the flying+sailing drone. Sections 3 and 4, respectively, present the implementation of the HMP for the minimization of the total control effort, and the minimization of the time required for the drone to reach the desired

10.1016/j.ifacol.2024.07.427

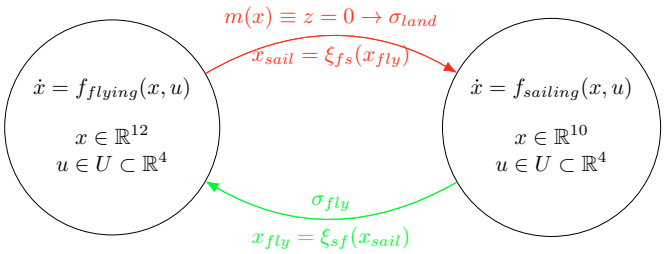

Fig. 1. The hybrid automata for flying+sailing drone with autonomous switching displayed in red arrows and controlled switching displayed in green.

terminal state. Numerical simulations are presented in Section 5. Conclusion and future research directions are discussed in Section 6.

2. HYBRID SYSTEMS MODELING OF THE DRONE

2.1 Hybrid Systems Structure

Following (Pakniyat and Caines, 2017b, 2021, 2023), a *hybrid system (structure)* $\mathbb{H}$ is considered as a septuple

$$\mathbb{H} = \{H, I, \Gamma, A, F, \Xi, \mathcal{M}\}, \tag{1}$$

where $H := \coprod_{q\in Q} \mathbb{R}^{n_q}$ is the hybrid state space with $|Q| < \infty$; in this article, $Q = \{q_1, q_2\} \equiv \{flying, sailing\}$, with $n_{q_1} = 12$ and $n_{q_2} = 10$.

$I := \Sigma \times U$ is the input value set with $|\Sigma| < \infty$, and $U \subset \mathbb{R}^m$; where, for flying+sailing drone, $\Sigma = \{\sigma_{fly}, \sigma_{land}\}$ and $U \subseteq \mathbb{R}^4$, with σ_{fly} corresponding to a controlled switching command and σ_{land} an autonomous switching.

$\Gamma : H \times \Sigma \to H$ is a *discrete state transition map* which, for the flying+sailing drone, is displayed as part of Fig. 1.

$A : Q \times \Sigma \to Q$ is the automaton's transition function on the state space Q and event set Σ, as displayed in Fig. 1.

$F := \{f_q\}_{q\in Q}$ is an indexed collection of measurable functions whose elements are presented in Section 2.2.

$\Xi : H \times \Sigma \to H$ is a family of continuous state jump transition maps which is presented in Section 2.2.

$\mathcal{M}$ is a collection of switching manifolds which is presented in Section 2.2.

2.2 Hybrid Optimal Control Problem

The nonlinear dynamics of the drone in flying mode is presented as

$$\dot{x}_{q_1} = f_{q_1}(x_{q_1}, u) \tag{2}$$

where the twelve-dimensional state space dynamics of the drone in the flying mode is expressed as (Sabatino, 2015)

$$\begin{aligned}
\dot{x}_1 &= x_2\\
\dot{x}_2 &= -\frac{(\sin x_7 \sin x_{11} + \cos x_7 \cos x_{11} \sin x_9)\, u_T}{m}\\
\dot{x}_3 &= x_4\\
\dot{x}_4 &= -\frac{(\cos x_7 \sin x_9 \sin x_{11} - \cos x_{11} \sin x_7) u_T}{m}\\
\dot{x}_5 &= x_6\\
\dot{x}_6 &= g - \frac{(\cos x_7 \cos x_9) u_T}{m}\\
\dot{x}_7 &= x_8\\
\dot{x}_8 &= \frac{I_y - I_z}{I_x} x_{10} x_{12} + \frac{1}{I_x} u_x\\
\dot{x}_9 &= x_{10}\\
\dot{x}_{10} &= \frac{I_z - I_x}{I_y} x_8 x_{12} + \frac{1}{I_y} u_y\\
\dot{x}_{11} &= x_{12}\\
\dot{x}_{12} &= \frac{I_x - I_y}{I_z} x_8 x_{10} + \frac{1}{I_z} u_z
\end{aligned} \tag{3}$$

subject to the initial condition $x_{q_1}(t_0) = x_0$, where m is the mass of the drone, g is the gravitational acceleration and I_x, I_y and I_z are inertia values around x, y, z axes, x_1, x_3 and x_5 are, respectively, the horizontal, lateral, and vertical positions of the drone, x_2, x_4 and x_6 are, respectively, the horizontal, lateral and vertical velocities. x_7, x_9 and x_{11} are, respectively, roll, pitch, and yaw angles, and x_8, x_{10}, and x_{11} are the rate of the angles respectively. u_T is the total thrust force produced by all rotors which are taking values from the set $[-10, +10]$ and u_x, u_y, and u_z are, respectively, the control torques generated by differences in the rotor's speeds which are taking values from the set $[-1, +1]$. The drone parameters are as Table 1.

The nonlinear dynamic of the drone in the sailing mode is written as

$$\dot{x}_{q_2} = f_{q_2}(x_{q_2}, u) \tag{4}$$

where the ten-dimensional state space dynamic of the drone in the sailing mode is expressed as

$$\begin{aligned}
\dot{x}_1 &= x_2\\
\dot{x}_2 &= -\frac{(\sin x_5 \sin x_9 + \cos x_5 \cos x_9 \sin x_7) u_T - \gamma_1 x_2^2}{m}\\
\dot{x}_3 &= x_4\\
\dot{x}_4 &= -\frac{(\cos x_5 \sin x_7 \sin x_9 - \cos x_9 \sin x_5) u_T - \gamma_2 x_4^2}{m}\\
\dot{x}_5 &= x_6\\
\dot{x}_6 &= \frac{I_y - I_z}{I_x} x_8 x_{10} + \frac{1}{I_x} u_x\\
\dot{x}_7 &= x_8\\
\dot{x}_8 &= \frac{I_z - I_x}{I_y} x_6 x_{10} + \frac{1}{I_y} u_y\\
\dot{x}_9 &= x_{10}\\
\dot{x}_{10} &= \frac{I_x - I_y}{I_z} x_6 x_8 + \frac{1}{I_z} u_z
\end{aligned} \tag{5}$$

where x_1 to x_4 are as before, and x_5 to x_{10} are as x_7 to x_{12} in the flying mode and γ_1 and γ_2 are drag coefficients along x and y, respectively. At the switching instant, the system's state before and after switching are related by the boundary condition

$$x_{q_2}(t_s) = \xi_{q_1 q_2}\big(x_{q_1}(t_s-)\big) \equiv \xi_{q_1 q_2}\Big(\lim_{t\to t_s} x_{q_1}(t)\Big) \tag{6}$$

where t_s indicates the time of the autonomous switching, when the drone finishes flying and begins sailing, and $\xi_{q_1 q_2}$ is the state transition jump map described by

$$x_{q_2} \equiv \begin{bmatrix} x_1(t_s)\\ x_2(t_s)\\ x_3(t_s)\\ x_4(t_s)\\ x_5(t_s)\\ x_6(t_s)\\ x_7(t_s)\\ x_8(t_s)\\ x_9(t_s)\\ x_{10}(t_s) \end{bmatrix} = \xi_{q_1 q_2}(x_{q_1}(t_s-)) = \begin{bmatrix} x_1(t_s-)\\ x_2(t_s-)\\ x_3(t_s-)\\ x_4(t_s-)\\ x_7(t_s-)\\ x_8(t_s-)\\ x_9(t_s-) + \delta\\ x_{10}(t_s-)\\ x_{11}(t_s-)\\ x_{12}(t_s-) \end{bmatrix} \tag{7}$$

where δ is the difference in the pitch angle between flying and sailing modes. The switching manifold which is the condition required to be satisfied for the flying mode to end and for the sailing mode to begin and corresponds to the drone landing over the water surface is expressed by $m_{q_1q_2}(x_{q_1}) = 0$, where $m_{q_1q_2}(x_{q_1}) = x_5 \equiv z$.

The objective of the associated hybrid optimal control problem (HOCP) is to minimize the hybrid cost

$$J = \int_0^{t_s} \ell_{q_1}\big(x_{q_1}(s), u(s)\big)ds + \int_{t_s}^{t_f} \ell_{q_2}\big(x_{q_2}(s), u(s)\big)ds \quad (8)$$

subject to $x_{q_2}(t_f) = x_f$, where ℓ_{q_1} and ℓ_{q_2} are cost functions associated with flying and sailing, respectively. In the problem of time minimization, the costs ℓ_{q_1}, ℓ_{q_2} are set to be equal to 1, and in the case of minimizing the control effort, these running cost functions are taken to be $\frac{1}{2}u^\top Ru$, where $R = R^\top > 0$.

3. THE MINIMUM CONTROL EFFORT PROBLEM

3.1 Hamiltonian minimization

The Hamiltonian for flying mode is written as

$$\begin{aligned} H_{q_1} &= \ell_{q_1} + \lambda_{q_1}^\top f_{q_1} = \frac{1}{2}u^\top Ru + \lambda_1 x_2 + \lambda_3 x_4 + \lambda_{11} x_{12} + \lambda_9 x_{10} \\ &- \lambda_2 \frac{(\sin x_7 \sin x_{11} + \cos x_7 \cos x_{11} \sin x_9)u_T}{m} + \lambda_5 x_6 \\ &- \lambda_4 \frac{(\cos x_7 \sin x_9 \sin x_{11} - \cos x_{11} \sin x_7)u_T}{m} + \lambda_7 x_8 \\ &+ \lambda_6\Big(g - \frac{(\cos x_7 \cos x_9)u_T}{m}\Big) + \lambda_8\Big(\frac{I_y - I_z}{I_x} x_{10}x_{12} + \frac{1}{I_x}u_x\Big) \\ &+ \lambda_{10}\Big(\frac{I_z - I_x}{I_y} x_8 x_{12} + \frac{1}{I_y}u_y\Big) + \lambda_{12}\Big(\frac{I_x - I_y}{I_z} x_8 x_{10} + \frac{1}{I_z}u_z\Big) \end{aligned} \quad (9)$$

and the Hamiltonian for sailing mode is expressed as

$$\begin{aligned} H_{q_2} &= \ell_{q_2} + \lambda_{q_2}^\top f_{q_2} = \frac{1}{2}u^\top Ru + \lambda_1 x_2 - \lambda_2 \gamma_1 x_2^2 + \lambda_3 x_4 \\ &- \lambda_2 \frac{(\sin x_5 \sin x_9 + \cos x_5 \cos x_9 \sin x_7)u_T}{m} - \lambda_4 \gamma_2 x_4^2 \\ &- \lambda_4 \frac{(\cos x_5 \sin x_7 \sin x_9 - \cos x_9 \sin x_5)u_T}{m} + \lambda_5 x_6 \\ &+ \lambda_6\Big(\frac{I_y - I_z}{I_x} x_8 x_{10} + \frac{1}{I_x}u_x\Big) + \lambda_7 x_8 + \lambda_9 x_{10} \\ &+ \lambda_8\Big(\frac{I_z - I_x}{I_y} x_6 x_{10} + \frac{1}{I_y}u_y\Big) + \lambda_{10}\Big(\frac{I_x - I_y}{I_z} x_6 x_8 + \frac{1}{I_z}u_z\Big) \end{aligned} \quad (10)$$

Thus the Hamiltonian minimization for flying mode yields

$$\frac{\partial H_{q_1}}{\partial u} = 0 \Rightarrow \begin{cases} u_T &= \lambda_2 \dfrac{\sin x_7 \sin x_{11} + \cos x_7 \cos x_{11} \sin x_9}{m} \\ &+ \lambda_4 \dfrac{\cos x_7 \sin x_9 \sin x_{11} - \cos x_{11} \sin x_7}{m} \\ &+ \lambda_6 \dfrac{\cos x_7 \cos x_9}{m} \\ u_x &= -\dfrac{1}{I_x}\lambda_8 \\ u_y &= -\dfrac{1}{I_y}\lambda_{10} \\ u_z &= -\dfrac{1}{I_z}\lambda_{12} \end{cases} \quad (11)$$

and for sailing mode, it yields

$$\frac{\partial H_{q_2}}{\partial u} = 0 \Rightarrow \begin{cases} u_T &= \lambda_2 \dfrac{\sin x_5 \sin x_9 + \cos x_5 \cos x_9 \sin x_7}{m} \\ &+ \lambda_4 \dfrac{\cos x_5 \sin x_7 \sin x_9 - \cos x_9 \sin x_5}{m} \\ u_x &= -\dfrac{1}{I_x}\lambda_6 \\ u_y &= -\dfrac{1}{I_y}\lambda_8 \\ u_z &= -\dfrac{1}{I_z}\lambda_{10} \end{cases} \quad (12)$$

3.2 Evolution of the adjoint process

The Hamiltonian canonical equation in the HMP yields the dynamics of the adjoint process for flying mode in $t \in [0, t_s]$ as

$$\begin{aligned} \dot\lambda_1 &= 0 \\ \dot\lambda_2 &= -\lambda_1 \\ \dot\lambda_3 &= 0 \\ \dot\lambda_4 &= -\lambda_3 \\ \dot\lambda_5 &= 0 \\ \dot\lambda_6 &= -\lambda_5 \\ \dot\lambda_7 &= -\lambda_2 \frac{(\cos x_7 \sin x_{11} - \sin x_7 \cos x_{11} \sin x_9)\, u_T}{m} \\ &+ \lambda_4 \frac{(\sin x_7 \sin x_9 \sin x_{11} + \cos x_{11} \cos x_7)u_T}{m} \\ &+ \lambda_6 \frac{(\sin x_7 \cos x_9)u_T}{m} \\ \dot\lambda_8 &= -\lambda_7 - \frac{I_z - I_x}{I_y}\lambda_{10}x_{12} - \frac{I_x - I_y}{I_z}\lambda_{12}x_{10} \\ \dot\lambda_9 &= -\lambda_2 \frac{(\cos x_7 \cos x_{11} \cos x_9)\, u_T}{m} \\ &- \lambda_4 \frac{(\cos x_7 \cos x_9 \sin x_{11})u_T}{m} + \lambda_6 \frac{(\cos x_7 \sin x_9)u_T}{m} \\ \dot\lambda_{10} &= -\lambda_9 - \frac{I_y - I_z}{I_x}\lambda_8 x_{12} - \frac{I_x - I_y}{I_z}\lambda_{12}x_8 \\ \dot\lambda_{11} &= -\lambda_2 \frac{(\sin x_7 \cos x_{11} - \cos x_7 \sin x_{11} \sin x_9)\, u_T}{m} \\ &- \lambda_4 \frac{(\cos x_7 \sin x_9 \cos x_{11} + \sin x_{11} \sin x_7)u_T}{m} \\ \dot\lambda_{12} &= -\lambda_{11} - \frac{I_y - I_z}{I_y}\lambda_8 x_{10} - \frac{I_z - I_x}{I_y}\lambda_{10}x_8 \end{aligned} \quad (13)$$

Furthermore, the dynamics of the adjoint process for sailing mode in $t \in [t_s, t_f]$ is written as

$$\begin{aligned} \dot\lambda_1 &= 0 \\ \dot\lambda_2 &= -\lambda_1 + \lambda_2 \gamma_1 x_2 \\ \dot\lambda_3 &= 0 \\ \dot\lambda_4 &= -\lambda_3 + \lambda_4 \gamma_1 x_4 \\ \dot\lambda_5 &= -\lambda_2 \frac{(\cos x_5 \sin x_9 - \sin x_5 \cos x_9 \sin x_7)u_T}{m} \\ &- \lambda_4 \frac{(-\sin x_5 \sin x_7 \sin x_9 - \cos x_9 \cos x_5)u_T}{m} \\ \dot\lambda_6 &= -\lambda_5 - \frac{I_z - I_x}{I_y}\lambda_8 x_{10} - \frac{I_x - I_y}{I_z}\lambda_{10}x_8 \\ \dot\lambda_7 &= -\lambda_2 \frac{(\cos x_5 \cos x_9 \cos x_7)u_T}{m} \\ &- \lambda_4 \frac{(\cos x_5 \cos x_7 \sin x_9)u_T}{m} \\ \dot\lambda_8 &= -\lambda_7 - \frac{I_y - I_z}{I_x}\lambda_6 x_{10} - \frac{I_x - I_y}{I_z} \end{aligned}$$

$$\dot{\lambda}_9 = -\lambda_2 \frac{(\sin x_5 \cos x_9 - \cos x_5 \sin x_9 \sin x_7)u_T}{m} - \lambda_4 \frac{(\cos x_5 \sin x_7 \cos x_9 + \sin x_9 \sin x_5)u_T}{m}$$
$$\dot{\lambda}_{10} = -\lambda_{11} - \frac{I_y - I_z}{I_y}\lambda_6 x_8 - \frac{I_z - I_x}{I_y}\lambda_8 x_6 \quad (14)$$

The boundary conditions for λ are determined from

$$\lambda_{q_1}(t_s) = \nabla \xi_{q_1 q_2}|^{\top}_{x_{q_1}(t_s-)} \lambda_{q_2}(t_s+) + p\, \nabla m|_{x_{q_1}(t_s-)} \quad (15)$$

4. THE MINIMUM TIME PROBLEM

4.1 Flying mode

The Hamiltonian for flying mode is written as

$$H_{q_1} = \ell_{q_1} + \lambda_{q_1}^{\top} f_{q_1} = 1 + \lambda_1 x_2 + \lambda_7 x_8 + \lambda_9 x_{10} + \lambda_{11} x_{12} - \lambda_2 \frac{(\sin x_7 \sin x_{11} + \cos x_7 \cos x_{11} \sin x_9)\, u_T}{m} + \lambda_3 x_4 - \lambda_4 \frac{(\cos x_7 \sin x_9 \sin x_{11} - \cos x_{11} \sin x_7)u_T}{m} + \lambda_5 x_6 + \lambda_6 \Big(g - \frac{(\cos x_7 \cos x_9)u_T}{m}\Big) + \lambda_8 \Big(\frac{I_y - I_z}{I_x} x_{10} x_{12} + \frac{1}{I_x} u_x\Big) + \lambda_{10} \Big(\frac{I_z - I_x}{I_y} x_8 x_{12} + \frac{1}{I_y} u_y\Big) + \lambda_{12} \Big(\frac{I_x - I_y}{I_z} x_8 x_{10} + \frac{1}{I_z} u_z\Big) \quad (16)$$

The Hamiltonian minimization for the Hamiltonian (16) yields the optimal values u_x^*, u_y^*, u_z^* and u_T^* , where for the input u_x we obtain

$$u_x^* = \underset{u_x \in [-1,+1]}{\operatorname{argmin}} \{\lambda_8 u_x\} \quad (17)$$

which takes the values -1 and $+1$ whenever λ_8 is, respectively, strictly positive and strictly negative. Hence, the control input u_x^* for time-optimal is given by

$$u_x^* = \begin{cases} +1 & \text{if } \lambda_8 < 0 \\ 0 & \text{if } \lambda_8 = 0 \\ -1 & \text{if } \lambda_8 > 0 \end{cases} \quad (18)$$

Similarly, for control inputs u_y we obtain

$$u_y^* = \begin{cases} +1 & \text{if } \lambda_{10} < 0 \\ 0 & \text{if } \lambda_{10} = 0 \\ -1 & \text{if } \lambda_{10} > 0 \end{cases} \quad (19)$$

and for control inputs u_z, we obtain

$$u_z^* = \begin{cases} +1 & \text{if } \lambda_{12} < 0 \\ 0 & \text{if } \lambda_{12} = 0 \\ -1 & \text{if } \lambda_{12} > 0 \end{cases} \quad (20)$$

Moreover, the control input u_T is obtained as

$$u_T^* = \underset{u_T \in [-10,+10]}{\operatorname{argmin}} \Big\{ \lambda_2 \frac{\sin x_7 \sin x_{11} + \cos x_7 \cos x_{11} \sin x_9}{m} u_T + \lambda_4 \frac{\cos x_7 \sin x_9 \sin x_{11} - \cos x_{11} \sin x_7}{m} u_T + \lambda_6 \frac{\cos x_7 \cos x_9}{m} u_T \Big\} \quad (21)$$

where the optimal input of u_T^* for flying mode, which depends on the sign of $\Delta = \lambda_2 \frac{\sin x_7 \sin x_{11} + \cos x_7 \cos x_{11} \sin x_9}{m} + \lambda_4 \frac{\cos x_7 \sin x_9 \sin x_{11} - \cos x_{11} \sin x_7}{m} + \lambda_6 \frac{\cos x_7 \cos x_9}{m}$, is determined by

$$u_T^* = \begin{cases} +10 & \text{if } \Delta \le 0 \\ -10 & \text{if } \Delta > 0 \end{cases} \quad (22)$$

It is worth mentioning that the control input u_T^* does not contain singular arcs, see, e.g., (Hehn et al., 2012, Section 3.1.2).

4.2 Sailing mode

The Hamiltonian for sailing mode is written as

$$H_{q_2} = \ell_{q_2} + \lambda_{q_2}^{\top} f_{q_2} = 1 + \lambda_1 x_2 - \lambda_2 \gamma_1 x_2^2 + \lambda_3 x_4 - \lambda_2 \frac{(\sin x_5 \sin x_9 + \cos x_5 \cos x_9 \sin x_7)u_T}{m} - \lambda_4 \gamma_2 x_4^2 - \lambda_4 \frac{(\cos x_5 \sin x_7 \sin x_9 - \cos x_9 \sin x_5)u_T}{m} + \lambda_7 x_8 + \lambda_6 \left(\frac{I_y - I_z}{I_x} x_8 x_{10} + \frac{1}{I_x} u_x\right) + \lambda_5 x_6 + \lambda_9 x_{10} + \lambda_8 \left(\frac{I_z - I_x}{I_y} x_6 x_{10} + \frac{1}{I_y} u_y\right) + \lambda_{10} \left(\frac{I_x - I_y}{I_z} x_6 x_8 + \frac{1}{I_z} u_z\right) \quad (23)$$

Similar to section 4.1 for control input u_x we obtain

$$u_x^* = \underset{u_x \in [-1,+1]}{\operatorname{argmin}} \{\lambda_6 u_x\} \quad (24)$$

which takes the values -1 and $+1$ whenever λ_6 is, respectively, strictly positive and strictly negative. Hence, the control input u_x^* for time-optimal is given by

$$u_x^* = \begin{cases} +1 & \text{if } \lambda_6 < 0 \\ 0 & \text{if } \lambda_6 = 0 \\ -1 & \text{if } \lambda_6 > 0 \end{cases} \quad (25)$$

Similarly, for control inputs u_y we obtain

$$u_y^* = \begin{cases} +1 & \text{if } \lambda_8 < 0 \\ 0 & \text{if } \lambda_8 = 0 \\ -1 & \text{if } \lambda_8 > 0 \end{cases} \quad (26)$$

and for control inputs u_z, we obtain

$$u_z^* = \begin{cases} +1 & \text{if } \lambda_{10} < 0 \\ 0 & \text{if } \lambda_{10} = 0 \\ -1 & \text{if } \lambda_{10} > 0 \end{cases} \quad (27)$$

In addition, the control input u_T is obtained as

$$u_T^* = \underset{u_T \in [-10,+10]}{\operatorname{argmin}} \Big\{ \lambda_2 \frac{\sin x_5 \sin x_9 + \cos x_5 \cos x_9 \sin x_7}{m} u_T + \lambda_4 \frac{\cos x_5 \sin x_7 \sin x_9 - \cos x_9 \sin x_5}{m} u_T \Big\} \quad (28)$$

Hence, the optimal input u_T^* for sailing mode depends on sign of $\Gamma = \lambda_2 \frac{\sin x_5 \sin x_9 + \cos x_5 \cos x_9 \sin x_7}{m} + \lambda_4 \frac{\cos x_5 \sin x_7 \sin x_9 - \cos x_9 \sin x_5}{m}$, is given by

$$u_T^* = \begin{cases} +10 & \text{if } \Gamma \le 0 \\ -10 & \text{if } \Gamma > 0 \end{cases} \quad (29)$$

5. NUMERICAL SIMULATION

We consider the values in Table 1 for the drone parameters with $x_{q_1}(t_0) = [0, 1, 0, 0, 10, 0.1, 0, 0, 0, 0, 1.5, 0]^{\top}$ as the initial condition in the flying mode, and a fixed terminal

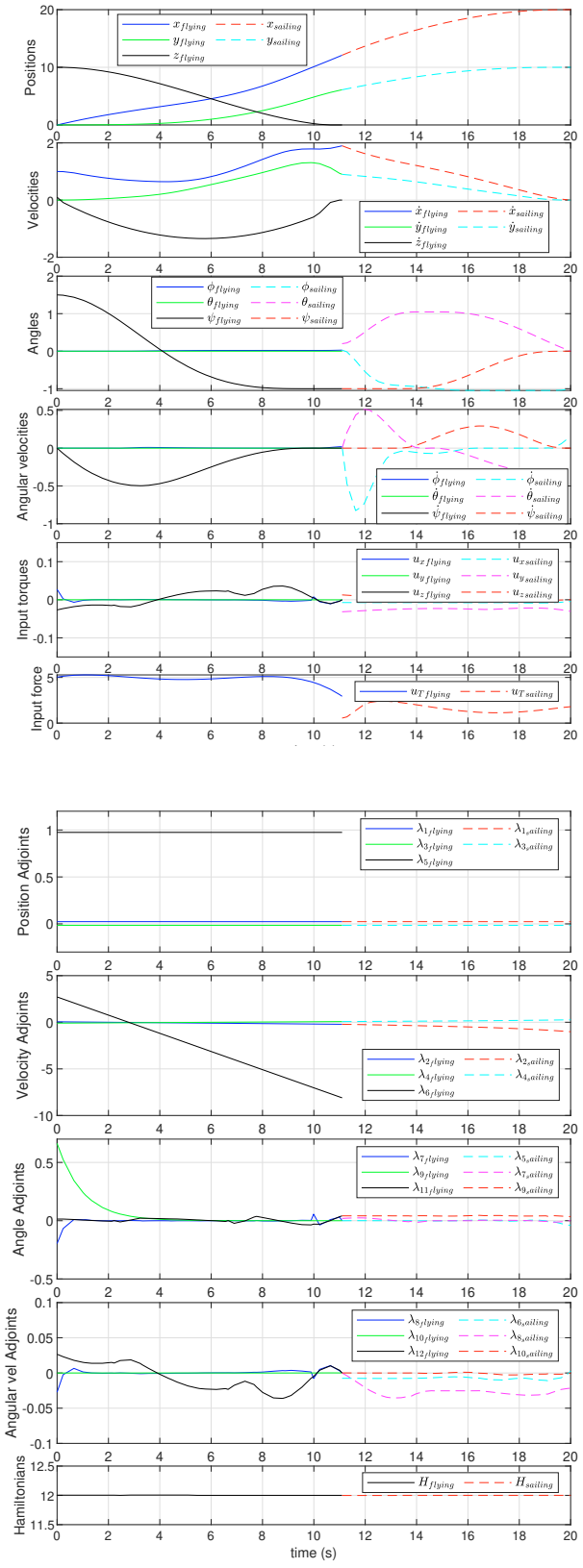

Fig. 2. The optimal trajectory (including positions, velocities, angles, angular velocities), the optimal inputs, the corresponding adjoint processes and Hamiltonians corresponding to the minimum control effort problem.

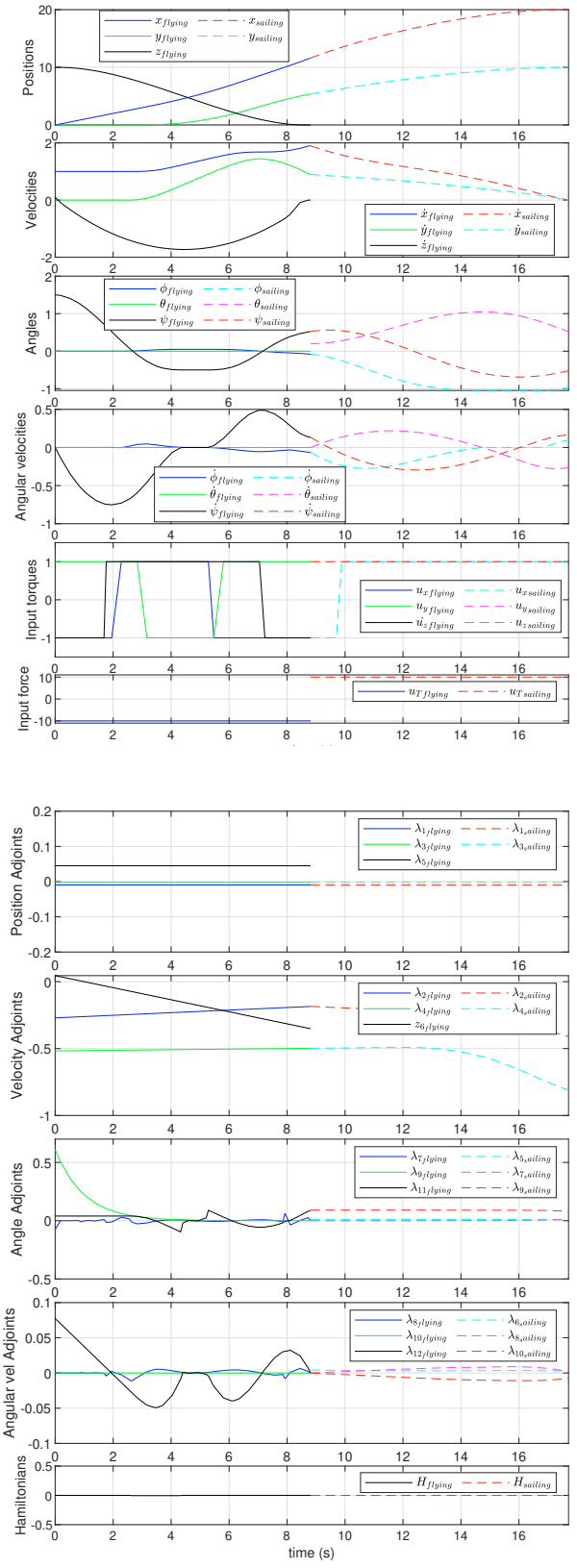

Fig. 3. The optimal trajectory (including positions, velocities, angles, angular velocities), the optimal inputs, the corresponding adjoint processes and Hamiltonians corresponding to the minimum time problem.

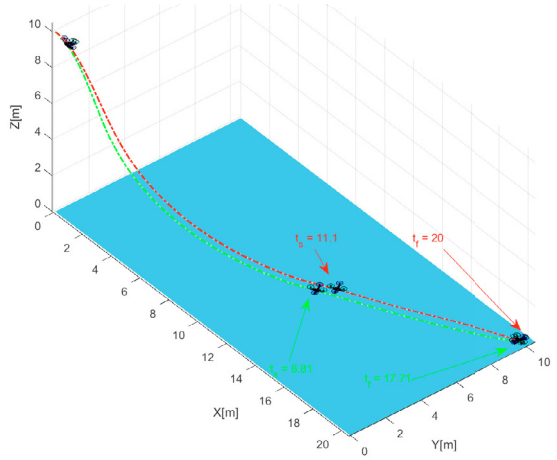

Fig. 4. The comparison of trajectories and switching times of the flying+sailing drone with optimal time (green) and optimal control effort (red).

Table 1. Values of the drone parameters (Sabatino, 2015).

Parameter	Value	Unit
m	0.5	kg
I_x	0.0034	Nms^2
I_y	0.0034	Nms^2
I_z	0.006	Nms^2
g	9.81	$\frac{m}{s^2}$

condition $x_{q_2}(t_f) = [20, 0, 10, 0, 0, 0, 0, 0, 0, 0, 0, 0]^\top$ on the water surface. We take $\delta = 25$ degrees for the instantaneous change in the pitch angle at the switching instance.

The results of the optimal control effort problem including states, adjoints, and Hamiltonians for the minimization of control effort throughout $[t_0, t_f] = [0, 20]$ are shown in Fig. 2. In this scenario, the optimal autonomous switching between flying and sailing modes occurs at $t_s = 11.1s$ at the optimal switching state $x_{q_1}(t_s-) = [12.13, 1.91, 3.62, 0.91, 0, 0.67, 0.02, 0.01, 0, 0.26, -.97, 0]^\top$.

The results for the time-optimal problem are shown in Fig. 3. The minimum terminal time is obtained as $t_f = 17.71s$ and the optimal switching time is $t_s = 8.81s$. In this solution, the optimal states at the switching instant are $x_{q_1}(t_s-) = [11.61, 1.9, 5.35, 0.9, 0, 0.54, -0.07, -0.06, 0, 0, 0.52, 0.13]^\top$.

The 3-D schematic view of a flying+sailing drone for optimal time and control effort problems is shown in Fig. 4.

6. CONCLUDING REMARKS

This paper presents a hybrid systems formulation of a robotic system capable of flying with 6-DoF and sailing with 5-DoF. The presented necessary optimality conditions of the HMP and the associated HMP–MAS algorithm for numerical simulations are powerful tools in providing solutions to the associated hybrid optimal control problems both for the minimization of time and the minimization of the control effort for the multi-modal robotic system. It shall be remarked, however, that due to the nonlinear nature of the drone dynamics, numerical solutions are sensitive to the initial guess, especially for the state components $x_7 \equiv \phi$, $x_9 \equiv \theta$, $x_{11} \equiv \psi$.

Future research directions include the accommodation of obstacle avoidance in the controller synthesis as well as the consideration of scenarios requiring a multiplicity of switchings. Another line of future work includes the implementation of these theoretical results on an actual flying+sailing drone as well as testing the multi-modal robotic system in real environments. An essential step in the practical implementation of the results is to establish separate hybrid modes for the transitioning of the drone from flying to sailing and vice versa based on the dynamics behavior of the corresponding robotic system.

REFERENCES

Ackerman, E. (2022). Darpa reincarnates soviet-era sea monster: Concept sea skimmer to fly meters above the ocean. *IEEE Spectrum*, 59(9), 6–13.

Hehn, M., Ritz, R., and D'Andrea, R. (2012). Performance benchmarking of quadrotor systems using time-optimal control. *Autonomous Robots*, 33, 69–88.

Ho, W.C., Shen, J.H., Liu, C.P., and Chen, Y.W. (2022). Research on optimal model of maritime search and rescue route for rescue of multiple distress targets. *Journal of Marine Science and Engineering*, 10(4), 460.

Pakniyat, A. and Caines, P.E. (2016). On the stochastic minimum principle for hybrid systems. In *2016 IEEE 55th Conference on Decision and Control (CDC)*, 1139–1144. IEEE.

Pakniyat, A. and Caines, P.E. (2017a). Hybrid optimal control of an electric vehicle with a dual-planetary transmission. *Nonlinear Analysis: Hybrid Systems*, 25, 263–282.

Pakniyat, A. and Caines, P.E. (2017b). On the relation between the minimum principle and dynamic programming for classical and hybrid control systems. *IEEE Transactions on Automatic Control*, 62(9), 4347–4362.

Pakniyat, A. and Caines, P.E. (2021). On the hybrid minimum principle: The hamiltonian and adjoint boundary conditions. *IEEE Transactions on Automatic Control*, 66(3), 1246–1253.

Pakniyat, A. and Caines, P.E. (2023). The minimum principle of hybrid optimal control theory. *Mathematics of Control, Signals, and Systems*, 1–50.

Qingqing, L., Taipalmaa, J., Queralta, J.P., Gia, T.N., Gabbouj, M., Tenhunen, H., Raitoharju, J., and Westerlund, T. (2020). Towards active vision with uavs in marine search and rescue: Analyzing human detection at variable altitudes. 65–70.

Sabatino, F. (2015). Quadrotor control: modeling, nonlinearcontrol design, and simulation.

Shaikh, M.S. and Caines, P.E. (2007). On the hybrid optimal control problem: theory and algorithms. *IEEE Transactions on Automatic Control*, 52(9), 1587–1603.

Sihite, E., Kalantari, A., Nemovi, R., Ramezani, A., and Gharib, M. (2023). Multi-modal mobility morphobot (m4) with appendage repurposing for locomotion plasticity enhancement. *Nature communications*, 14(1), 3323.

Yasini, T. and Pakniyat, A. (2023). Hybrid Optimal Control of a Flying+Sailing Drone. *ASME Letters in Dynamic Systems and Control*, 3(3), 031008.1–031008.7.